Journal of Electrical Systems and Information Technology xxx (2016) xxx–xxx
www.elsevier.com/locate/jesit

Design and control of a standalone PV water pumping system

Essam E. Aboul Zahab [a], Aziza M. Zaki [b], Mohamed M. El-sotouhy [b,*]

[a] Department of Electrical Power and Machines, Faculty of Engineering, Cairo University, Giza, Egypt
[b] Department of Power Electronics and Energy Conversion, Electronics Research Institute, Dokki, Giza, Egypt

Received 5 October 2015; received in revised form 22 February 2016; accepted 6 March 2016

Abstract

Water resources are vital for satisfying human needs. However, almost one-fifth of the world's population – about 1.2 billion people – live in areas where water is physically rare. One quarter of the global population also live in developing countries that face water shortages. This paper presents standalone PV water pumping system. Photovoltaic (PV) is the main power source, and lead acid batteries are used as energy storage system, to supply a water pump driven by a BLDC motor. The proposed control strategy consists of three control units. The first unit is to control the speed and hysteresis current controller for BLDC motor. The maximum power point tracking (MPPT) is the second control unit, and the battery charging/discharging system is controlled by the third controller. The simulation results show the effectiveness and the good efficiency of the proposed system.

Keywords: Photovoltaic (PV); Brushless direct current (BLDC); Perturb and observe (P&O); Fuzzy logic controller (FLC); Alternative current (AC); Direct current (DC); State of charge (SOC)

1. Introduction

Water resources are vital for satisfying human needs, protecting health, and guaranteeing food production energy and the rebuilding of ecosystems, as well as for social and economic development and for sustainable development. However, according to UN World Water Development Report in 2015, almost one-fifth of the world's population (about 1.2 billion people) live in zones where water is physically rare. One quarter of the global population also live in developing countries that face water shortages (The United Nations World Water Development Report, 2015). Remote water pumping systems are a basic choice in meeting this need. Installation of a new transmission line and a transformer to the remote areas is often very expensive (Hmidet et al., 2014). Also the costs of fossil fuels and their environmental impacts rise, the demand for renewable energy sources increases (Aashoor and Robinson, 2013; Sreekumar and Benny, 2013). If the source of water is 1/3 mile (app. 0.53 km) or more away from the power line,

* Corresponding author.
E-mail address: mohamedmostafa_87@yahoo.com (M.M. El-sotouhy).
Peer review under the responsibility of Electronics Research Institute (ERI).

Production and hosting by Elsevier

http://dx.doi.org/10.1016/j.jesit.2016.03.003

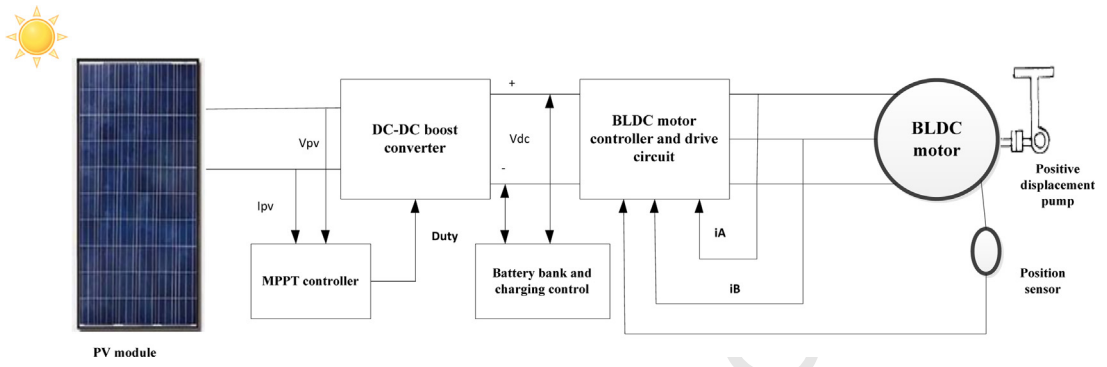

Fig. 1. The proposed system.

photovoltaic (PV) is preferred as an economic choice (Oi, 2005). There are many techniques for maximizing the output power from the PV modules either conventional techniques like perturb and observe (P&O) or intelligent techniques like fuzzy control (Sreekumar and Benny, 2013). The photovoltaic pumping has turn out to be one of the most favorable fields in photovoltaic applications. For a standalone PV system there are mainly two types of pumps: centrifugal and positive displacement pumps. In the centrifugal pump, the rotation of an impeller forces water into the tube. The water speed and pressure depend on the available mechanical power at the rotating impeller and the total head, but the displacement pump uses a piston or a screw to control the water flow. The positive displacement pump grants a better efficiency under low power conditions than the centrifugal pump. The water pumps may be driven by many types of driving systems. The more popular are direct current (DC) motors, alternative current (AC) motors or BLDC motors (Mohammedi et al., 2013). Brushless DC (BLDC) motor drives have received wide care as their performance is superior to those of conventional brushed DC motors and AC motors. In small units up to 5.0 kW, BLDC motors are preferable and have increased the request in water pumping systems operated by a photovoltaic array because of their higher operating efficiency and good starting torque (Putta Swamy et al., 1995). Hysteresis current control is one of the simple PWM current control techniques which are used for minimizing commutation torque ripple, and are easy to implement (Das and Chanda, 2014). As photovoltaic produces electricity only when the sunlight exists, so stand alone PV systems need a backup energy storage which makes it available through the bad weather or night conditions. In standalone PV systems, among many possible storage mediums, batteries are commonly used as a storage element. The lead-acid battery is most common used with standalone PV systems because it is quite cheap and broadly available (Jaycar Electronics Reference Data Sheet, 2016). This paper presents an efficient PV water pumping system. It provides theoretical studies and modeling for all the system components, comparison between (P&O) & fuzzy maximum power point techniques, and provides the motor performance (speed, torque, etc.) results.

2. The proposed system

The stand-alone PV water pumping system consists of a single PV module of 300 W rating, a maximum power point tracking, a battery bank with charging controller, BLDC motor driving a positive displacement pump, and BLDC motor controller as shown in Fig. 1.

2.1. PV module model

There are various sizes of PV module available in the market. Usually, a number of PV modules are combined as an array (either series or parallel connection) to meet different energy demands. The size of the PV module selected for the proposed system is 300 W module. The selected module is IS4000P 300 W multi-crystalline PV module. As shown in Fig. 2, the model of the PV module can be represented as shown in the equivalent circuit (Fig. 2) as a current source in parallel with a diode (Mahmoud et al., 2012).

Please cite this article in press as: Aboul Zahab, E.E., et al., Design and control of a standalone PV water pumping system. J. Electr. Syst. Inform. Technol. (2016), http://dx.doi.org/10.1016/j.jesit.2016.03.003

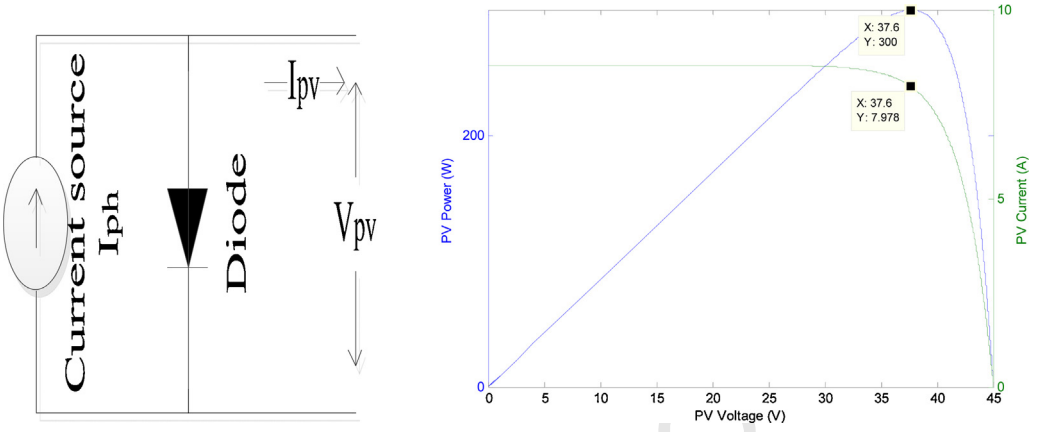

Fig. 2. The PV model and its simulated electrical characteristics.

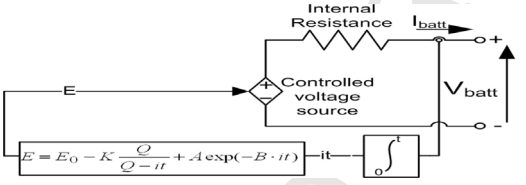

Fig. 3. General model of battery.

The PV cell electrical characteristics are nonlinear and vary according to the solar insolation (G) and the cell temperature (T). The PV output current I_{pv} can be stated by Eq. (1).

$$I_{pv} = I_{ph} - I_0(e^{(\frac{q \times V_{pv}}{nKT})} - 1) \quad (1)$$

where I_{pv} is the output current from the PV cell, I_{ph} is the photo generated current, I_0 is the saturation current in the dark, q is the electron charge = 1.6×10^{-19} (C), V_{pv} is the output voltage of the PV cell, n is the diode ideality factor, K is Boltzmann constant = 1.38×10^{-23} (J/K), T is the cell temperature (°C). The PV module output current of a number of cells connected in series (N_s) and number of cells connected in parallel (N_p) can be stated by Eq. (2).

$$I_{pv} = N_p I_{ph} - N_p I_0(e^{(\frac{q \times V_{pv}}{N_s \times n \times K \times T})} - 1) \quad (2)$$

The simulated electrical characteristics of the adopted PV module at standard conditions (irradiance = 1000 W/m^2 &temperature = 25 °C) are shown in Fig. 2.

2.2. Battery model

The batteries are used for store the excess power and supply it to the load in bad weather conditions or in night periods. In the standalone photovoltaic systems the commercial rechargeable batteries in the market are: lead-acid or (Pb-S), the nickel-cadmium or (NiCad), the nickel-metal hydride or (NiMH), and the lithium-ion or (Li-ion) types. Lead-acid batteries are the most popular, and widely used in renewable energy systems. The equivalent circuit of a general battery dynamic model parameterized to characterize most popular types of rechargeable batteries. This model can be represented by a simple controlled voltage source in series with a constant resistance, as shown in Fig. 3, and described by Eqs. (3) & (4) (Tremblay et al., 2007).

$$E = E_0 - K\frac{Q}{Q - \int i\mathrm{d}t} + A\exp(-B\int i\mathrm{d}t) \quad (3)$$

$$V_{bat.} = E - i \times R \quad (4)$$

where E is the no-load voltage (V), E_0 is the battery constant voltage = 12 V, K is the polarization voltage (V), Q is the battery capacity (Ah), $\int i\mathrm{d}t$ is the actual battery charge (Ah), A is the exponential zone amplitude (V), B is the

Please cite this article in press as: Aboul Zahab, E.E., et al., Design and control of a standalone PV water pumping system. J. Electr. Syst. Inform. Technol. (2016), http://dx.doi.org/10.1016/j.jesit.2016.03.003

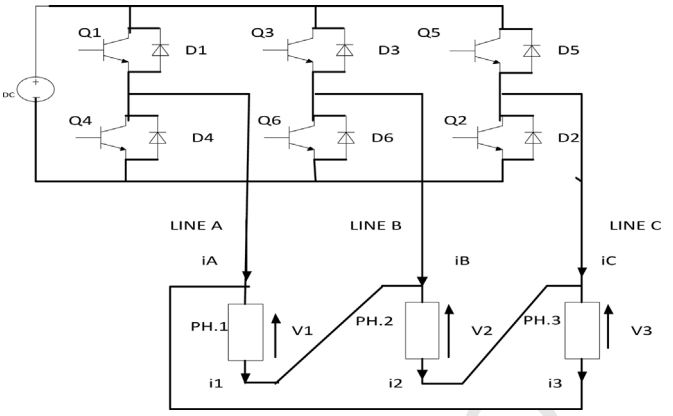

Fig. 4. Circuit diagram of delta connected motor.

exponential zone time constant inverse $(\mathrm{Ah})^{-1}$, V_{bat} is the battery voltage (V), R is the internal resistance (ohm), i is the battery current (A).

2.3. BLDC motor model

Three phase BLDC motor connection may be star or delta connected, the motor used in the simulation is delta connected as shown in Fig. 4.

The line to line voltages and BEMFs are the same as phase voltages and BEMFs (Pillay and Krishnan, 1989a,b). Suppose Lab = Lbc = Lca = L, and Rab = Rbc = Rca = R.

$$V_1 = i_1 R + L\left(\frac{\mathrm{d}i_1}{\mathrm{d}t}\right) + e_1 \tag{5}$$

$$V_2 = i_2 R + L\left(\frac{\mathrm{d}i_2}{\mathrm{d}t}\right) + e_2 \tag{6}$$

$$V_3 = i_3 R + L\left(\frac{\mathrm{d}i_3}{\mathrm{d}t}\right) + e_3 \tag{7}$$

where L is the armature self-inductance [H], R is the armature resistance [Ω], V_{a}, V_{b}, V_{c} are the terminal phases or lines voltages [V], i_1, i_2, i_3 are motor input currents [A], and e_1, e_2, e_3 are motor back-EMFs [V]. In the 3-phase BLDC motor, the back-EMF is related to a function of the rotor position and the back-EMF of each phase has 120° phase angle difference so the equation of each phase should be as follows:

$$e_{\mathrm{a}} = K_{\mathrm{w}} f(\theta_{\mathrm{e}})\omega \tag{8}$$

$$e_{\mathrm{b}} = K_{\mathrm{w}} f(\theta_{\mathrm{e}} - 120)\omega \tag{9}$$

$$e_{\mathrm{c}} = K_{\mathrm{w}} f(\theta_{\mathrm{e}} - 240)\omega \tag{10}$$

$$e_1 = e_{\mathrm{a}} - e_{\mathrm{b}} \tag{11}$$

$$e_2 = e_{\mathrm{b}} - e_{\mathrm{c}} \tag{12}$$

$$e_3 = e_{\mathrm{c}} - e_{\mathrm{a}} \tag{13}$$

where K_{w} is the back EMF constant of one phase [V/rad s^{-1}], θ_{e} is the electrical rotor angle [°el.], ω is the rotor speed [rad s^{-1}], e_{a}, e_{b}, e_{c} are trapezoidal functions with 120° flat top, the electrical rotor angle is equal to the mechanical rotor angle multiplied by the number of pole pairs p:

$$\theta_{\mathrm{e}} = \left(\frac{p}{2}\right)\theta_{\mathrm{m}} \tag{14}$$

where θ_m is the mechanical rotor angle [rad].

The function $F(\theta_e)$ gives the trapezoidal waveform of the back-emf. One period of this function can be written as:

$$f(\theta_e) = \begin{cases} 1 & 0 \le \theta < \frac{2\pi}{3} \\ 1 - \frac{6}{\pi}\left(\theta_e - \frac{2\pi}{3}\right) & \frac{2\pi}{3} \le \theta < \pi \\ -1 & \pi \le \theta < \frac{5\pi}{3} \\ -1 + \frac{6}{\pi}\left(\theta_e + \frac{2\pi}{3}\right) & \frac{5\pi}{3} \le \theta < 2\pi \end{cases} \quad (15)$$

Total torque output can be represented as the summation of that of the 3 phases. Next equation represents the total output torque in [Nm]:

$$T = \frac{e_a i_a + e_b i_b + e_c i_c}{\omega} \quad (16)$$

The mechanical equation of the motor is as follows:

$$Te - Tl = J\left(\frac{d\omega}{dt}\right) + \beta\omega \quad (17)$$

So the motor speed can be calculated as:

$$\omega = \int \frac{(Te - Tl - \beta\omega)}{J} \quad (18)$$

where Tl is the pump load torque [Nm], J is the inertia of rotor and coupled shaft [kg m^2], β is the friction constant [Nm s rad-1]. Then the rotor position is calculated by integrating the speed of the motor, and then we could calculate the phase currents and line currents by applying Kirchhoff's law at three nodes (a–c). These line currents are feedback to the hysteresis current control to get the state of the transistors.

3. Control strategy

In this work the control strategy is divided into three main control units. (1) First control unit is responsible for speed and hysteresis current control for the BLDC motor pump, (2) second control unit is responsible for MPPT, and (3) third control unit is responsible for charging and discharging of the battery bank.

3.1. Speed and hysteresis current control for the BLDC motor pump

Fig. 5 describes the basic blocks of the PMBLDCM drive. The drive contains speed controller, reference current generator, PWM current controller, position sensor, the motor and the inverter. The purpose of a motor speed controller is to yield a signal representing the required speed, and to drive a motor at that speed. Speed controller calculates the difference between the reference speed and the real speed producing an error, which is fed to the PI controller. The parameters of the PI controllers are obtained by using trial and error method. PI controllers are used widely for motion control systems. The controller tries to minimize the error by adjusting the process control inputs. Here the proposed technique consists of the outer speed loop and one inner current loop as the double-loop control system is introduced, shown in Fig. 5. In the double-loop control system, a PI controller is adopted in the speed loop and a hysteresis current controller is adopted in the current loop on the principle of hysteresis current track current controlled voltage source inverter (Sanita and Kuncheria, 2013). Hysteresis current control is one of the simple PWM current control techniques which are used for minimizing commutation torque ripple, and it is easy to implement. This simple control strategy will be presented at low cost and uses simple structure and requires minor memory or processing abilities. This type of BLDC drive is very suitable for renewable applications. Although hysteresis control is insensitive to motor parameter variations, the stability of its normal operations has to be confirmed (Das and Chanda, 2014).

Please cite this article in press as: Aboul Zahab, E.E., et al., Design and control of a standalone PV water pumping system. J. Electr. Syst. Inform. Technol. (2016), http://dx.doi.org/10.1016/j.jesit.2016.03.003

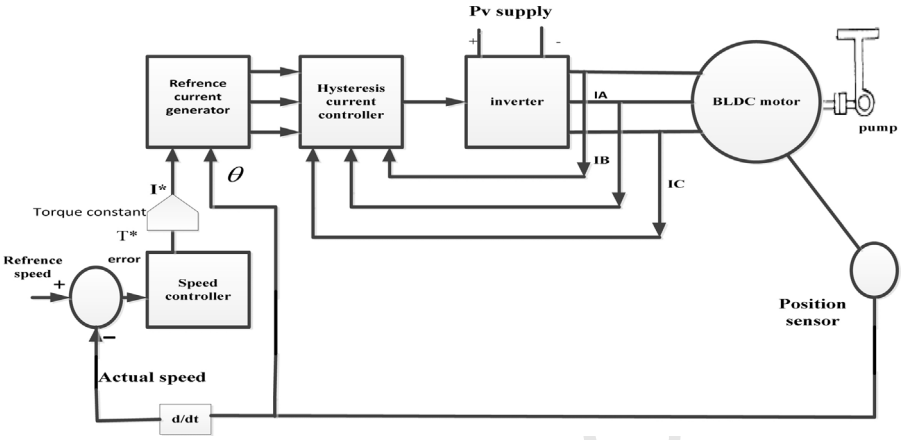

Fig. 5. The basic blocks of the BLDC motor drive.

Table 1
Q8 The reference current depending on rotor position.

Rotorposition (θ)	Referencecurrents		
	I^*_a	I^*_b	I^*_c
$0 \le \theta < \pi/3$	Is	−Is	0
$\pi/3 \le \theta < 2\pi/3$	Is	0	−Is
$2\pi/3 \le \theta < \pi$	0	Is	−Is
$\pi \le \theta < 4\pi/3$	−Is	Is	0
$4\pi/3 \le \theta < 5\pi/3$	−Is	0	Is
$5\pi/3 \le \theta < 2\pi$	0	−Is	Is

Table 2
Hysteresis current control logic (Putta Swamy et al., 1995).

ΔIx	Switch					
	Q1	Q2	Q3	Q4	Q5	Q6
ΔIA > h	ON	OFF	OFF	OFF	OFF	OFF
ΔIA < −h	OFF	OFF	OFF	ON	OFF	OFF
ΔIB > h	OFF	OFF	ON	OFF	OFF	OFF
ΔIB < −h	OFF	OFF	OFF	OFF	OFF	ON
ΔIC > h	OFF	OFF	OFF	OFF	ON	OFF
ΔIC < −h	OFF	ON	OFF	OFF	OFF	OFF

3.3.1. *Reference current generator*

The input signals needed for generating the reference currents (I^*_a, I^*_b, I^*_c) are the rotor position (θ), and the magnitude of the three phase currents (I^*) generated from Eq. (19):

$$I^* = \frac{T^*}{K_t} \tag{19}$$

where K_t is the torque constant, T^* is the reference torque value generated from the PI speed controller. The reason that this is called a hysteresis controller is that the phase voltage switches to retain the phase currents within the hysteresis bands. The hysteresis band has a width equal *2* h. Hysteresis current control can be implemented by computing reference current I^*_x as shown in Table 1 and measuring the actual current I_x where $x = a$, b, or c and then calculate error signal $\Delta I_x = I^*_x - I_x$ and then apply the logic shown in Table 2, which activate the switches shown above in Fig. 5. The reference current values can be created with respect to the rotor position as shown in Table 1 (Putta Swamy et al., 1995; Pillay and Krishnan, 1989a).

Please cite this article in press as: Aboul Zahab, E.E., et al., Design and control of a standalone PV water pumping system. J. Electr. Syst. Inform. Technol. (2016), http://dx.doi.org/10.1016/j.jesit.2016.03.003

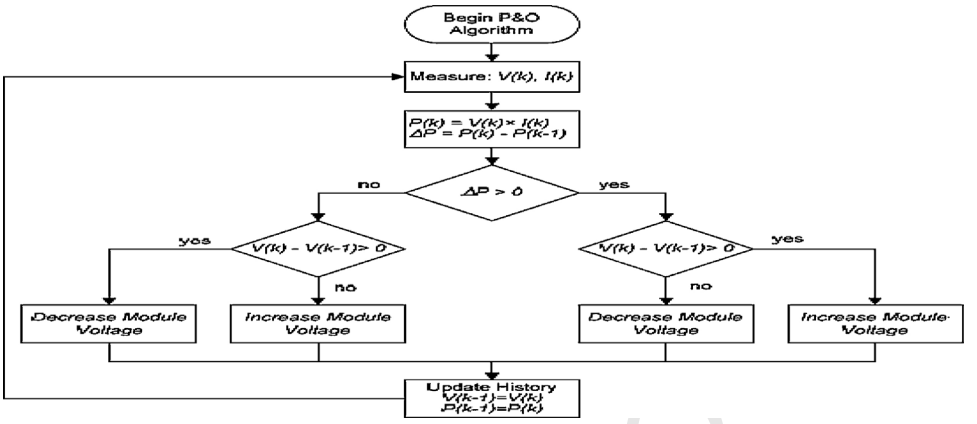

Fig. 6. Perturb and observe algorithm (P&O) (Oi, 2005).

The hysteresis current controller gives the switching of 6 switches to the inverter devices shown up in Fig. 4. The switching logic is formulated as given in Table 2.

3.2. The MPPT control unit

The MPPT control unit is used to keep the output power of the PV as maximum as possible. This control unit is implemented using two MPPT algorithms: (1) P&O and (2) FLC as follows:

3.2.1. P&O algorithm

In this method the PV output current and voltage are measured (I_{pv}, V_{pv}), and the operating voltage (V_{pv}) is perturbed (increased) by a small decrease in the duty cycle D by a rate (dD) of the boost converter and observing the change in power and the change in voltage then calculate the (dP/dV) value. If (dP/dV) is positive the perturbation of the operating voltage will be in the same way of increasing so should continue decreasing the duty cycle of the boost converter. If dP/dV is negative the operating voltage should be perturbed in the reverse direction (decreased). The maximum power point is obtained when dP/dV = 0. The flowchart of this algorithm is shown in Fig. 6. (Oi, 2005; Elgendy et al., 2012).

3.2.2. FLC based MPPT algorithm

Fuzzy logic control (FLC) is used largely in control engineering and is very important when there is no exact mathematical model or while the controlled process is nonlinear (Rebhi et al., 2013). Fuzzy logic controller has been largely used for industrial processes in the recent years due to its simplicity and effectiveness for both linear and non-linear systems. It consists of three blocks: Fuzzification, Fuzzy rules and inference engine, and finally Defuzzification (Aashoor and Robinson, 2013).

3.2.2.1. Fuzzification. In the fuzzification stage, numerical input variables are transformed into linguistic variables based on subsets called membership function. The proposed fuzzy logic controller has two input variables dP_{pv} & dI_{pv},and one output variable dD:

$$\mathrm{d}P_{pv} = P_{pv}(k) - P_{pv}(k-1) \tag{20}$$

$$\mathrm{d}I_{pv} = I_{pv}(k) - I_{pv}(k-1) \tag{21}$$

$$\mathrm{d}D = D(k) - D(k-1) \tag{22}$$

where dP is the change in PV power, dI is the change in PV current and dD is the change in duty cycle. Fig. 7 shows the membership functions of the two inputs and the output fuzzy sets. Each fuzzy set has four membership functions as follows: PB (Positive Big), PS (Positive Small), NS (Negative Small) and NB (Negative Big).

Please cite this article in press as: Aboul Zahab, E.E., et al., Design and control of a standalone PV water pumping system. J. Electr. Syst. Inform. Technol. (2016), http://dx.doi.org/10.1016/j.jesit.2016.03.003

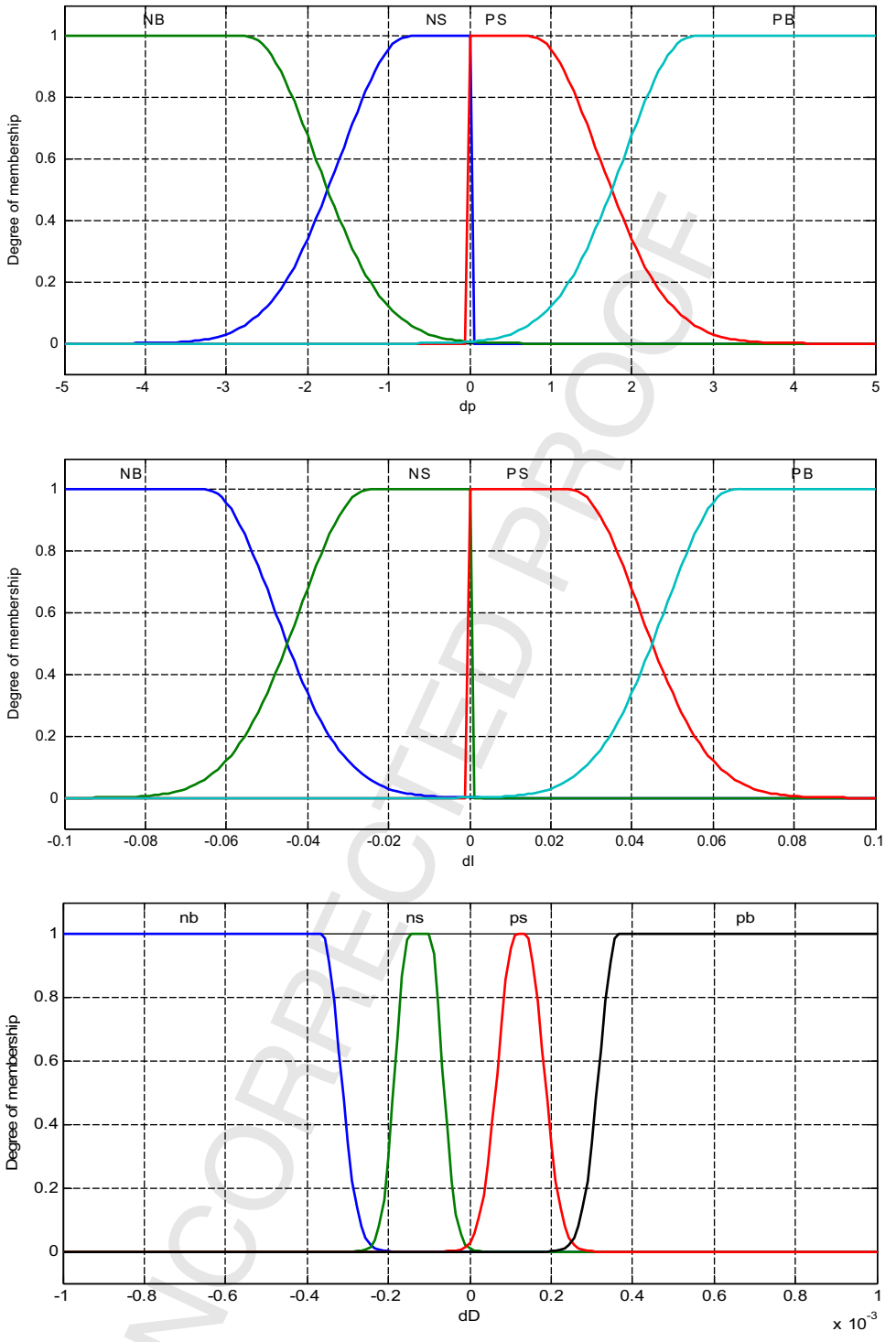

Fig. 7. Inputs and output of fuzzy sets.

Table 3
Fuzzy rules.

d*I*	d*P*			
	PB	PS	NS	NB
PB	PB	PS	NS	NB
PS	PB	PS	NS	NB
NS	NB	NS	PS	PB
NB	NB	NS	PS	PB

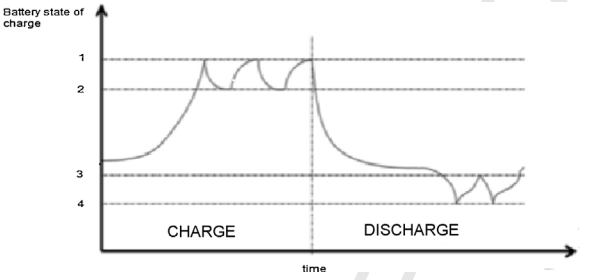

Fig. 8. Intermittent charging & discharging control.

3.3.2.2. Fuzzy rules and inference engine. Fuzzy rules include a set of rules in linguistic form which subordinate the fuzzy inputs with the fuzzy output. These are created by an expert knowledge and understanding of the system performance that is essential to realize the control objectives. The fuzzy control rules have been established using a set of IF-THEN rules as defined in Table 3.

3.2.2.3. Defuzzification. In the defuzzification step the output of fuzzy logic control is converted from linguistic variables to numerical variables, where in this process the crisp output of the FLC (d*D*) is calculated. There are different approaches for defuzzifying a result fuzzy set. The method used in this paper is called the Center of Gravity (Aashoor and Robinson, 2013). FLC can track the MPP rapidly with small oscillations around it (Mansour et al., 2015).

3.3. The battery bank charging and discharging control technique

There are many battery charging algorithms used to keep the battery at a high state of charge and increase the life time of the battery. The intermittent charging control is the most generally used technique in commercial chargers (Armstrong et al., 2008). In the charging mode, the battery is charged with maximum power point tracking (MPPT) between two predefined voltage edges as shown in Fig. 8. When the battery reaches the upper voltage edge, at point 1, the charging is stopped, then the battery voltage is observed until it drops to the lower voltage edge, at point 2, then the charging begins again. The same process is repeated at the discharging mode process to protect the battery bank from deep discharging, when the battery voltage reaches the edge point 4 the discharge from battery bank should stop, and repeat discharging from batteries after their voltage become larger than or equal to the voltage at edge point 3. So, we could protect the battery bank from overcharging and deep discharging.

4. Simulation results

The system is simulated in the MATLAB/SIMULINK program with sample time equal to two micro seconds using two MPPT techniques (P&O, and fuzzy) using the same motor control (outer speed control, inner hysteresis current controller).

Please cite this article in press as: Aboul Zahab, E.E., et al., Design and control of a standalone PV water pumping system. J. Electr. Syst. Inform. Technol. (2016), http://dx.doi.org/10.1016/j.jesit.2016.03.003

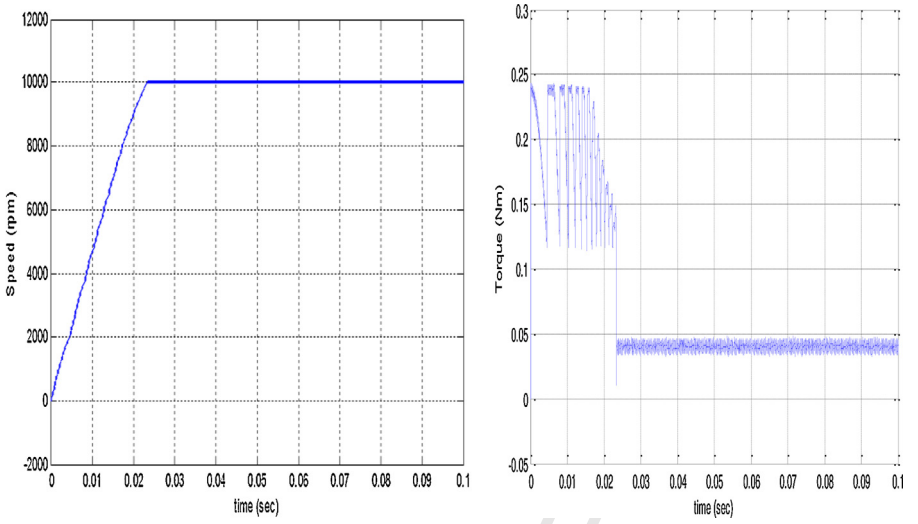

Fig. 9. Motor rated speed and rated torque.

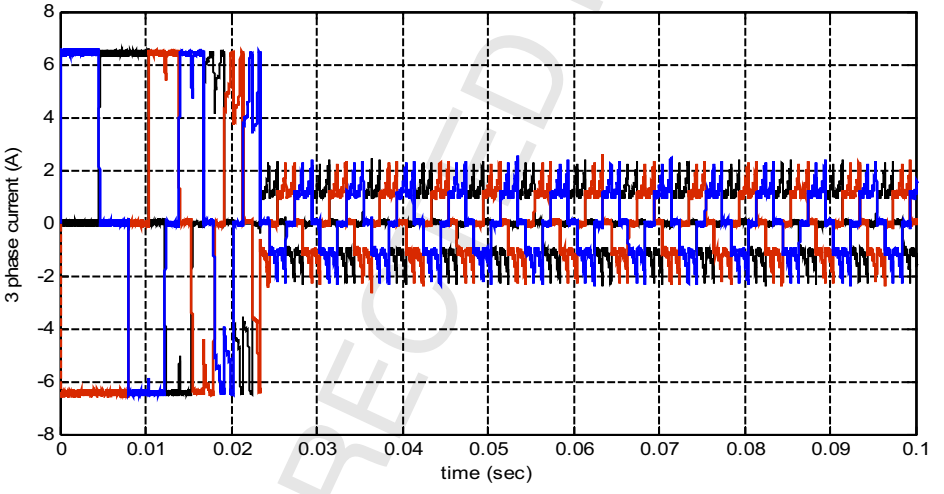

Fig. 10. Motor three phase rated currents.

4.1. BLDC motor pump simulation results

Suppose the motor works at nominal speed and at nominal voltage as in Appendix A. The rated speed and rated torque, the three phase currents, rotor position, and BEMFs are shown in Figs. 9–12 respectively.

4.2. MPPT simulation results using P&O technique

Suppose the module temperature is constant at 25 °C and the irradiance is variable and change through a day as (0.4, 0.6, 0.7, 0.8, 0.9, 1, 0.9, 0.8, 0.7, and 0.3), and the step change in duty cycle is dD = 0.001. The results show the output module power through a day (represented in simulation time by one second) in Fig. 13 using P&O MPPT technique.

Please cite this article in press as: Aboul Zahab, E.E., et al., Design and control of a standalone PV water pumping system. J. Electr. Syst. Inform. Technol. (2016), http://dx.doi.org/10.1016/j.jesit.2016.03.003

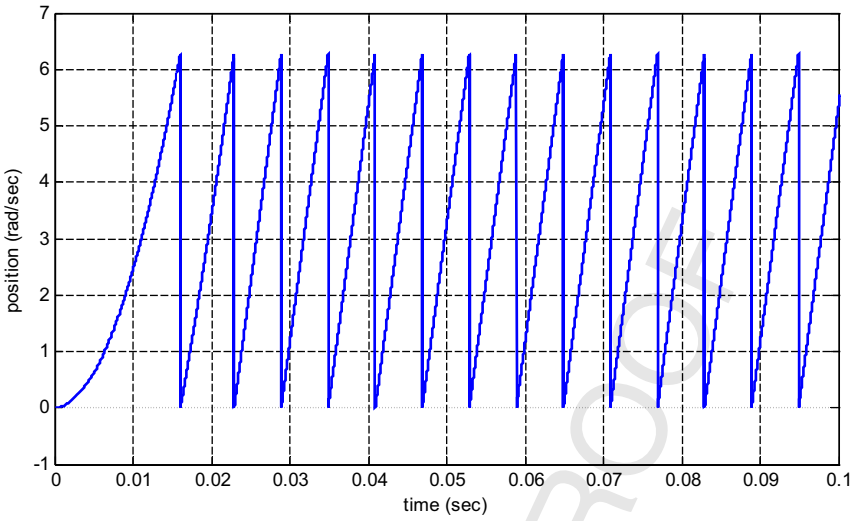

Fig. 11. Motor rotor positions.

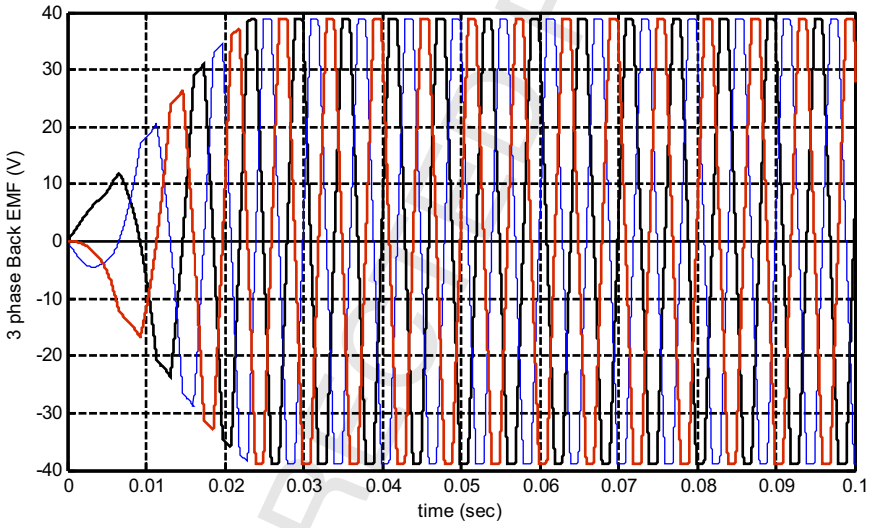

Fig. 12. Motor three BEMFs.

4.3. MPPT simulation results using fuzzy technique

Suppose the module temperature is constant at 25 °C and the irradiance is variable and change through day as (0.4, 0.6, 0.7, 0.8, 0.9, 1, 0.9, 0.8, 0.7, and 0.3). The results show the output module power through a day (represented in simulation time by one second) with MPPT using fuzzy intelligent techniques shown in Fig. 14.

4.4. Simulation results of battery intermittent charging control algorithm

The intermittent charging control has two bands to protect the battery from over charging where batteries SOC supposed (98:100%) and lower band to protect the batteries from the deep discharging where batteries SOC supposed (25:20%).

Suppose the batteries initial state of charge (SOC) is 30%, and the weather is bad or at night, then the batteries discharge until the SOC becomes ≤20% (at point 4) here stop the discharge process by switching off a switch supposed it (s2). And when the battery recharges again, the supposed switch (s2) becomes ON but after the SOC reaches ≥25%

Please cite this article in press as: Aboul Zahab, E.E., et al., Design and control of a standalone PV water pumping system. J. Electr. Syst. Inform. Technol. (2016), http://dx.doi.org/10.1016/j.jesit.2016.03.003

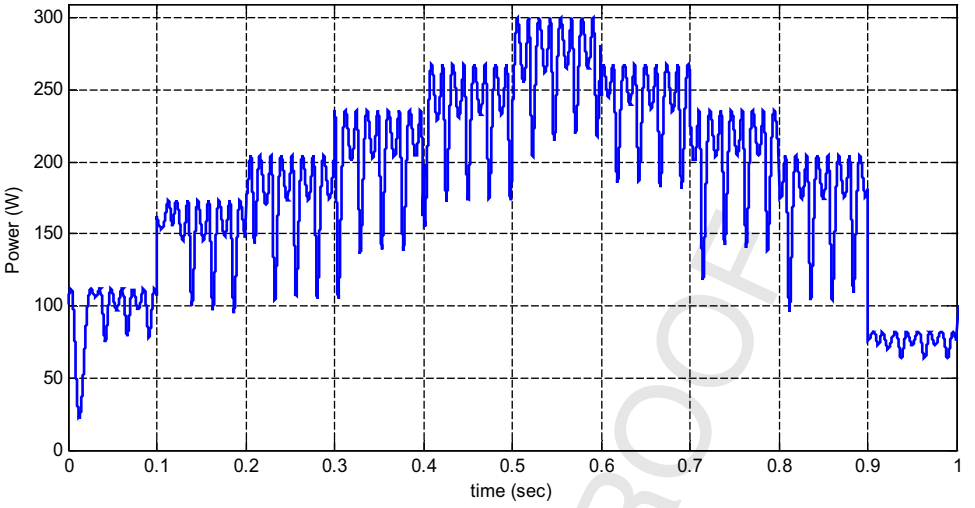

Fig. 13. Module output power through a day with MPPT using P&O technique.

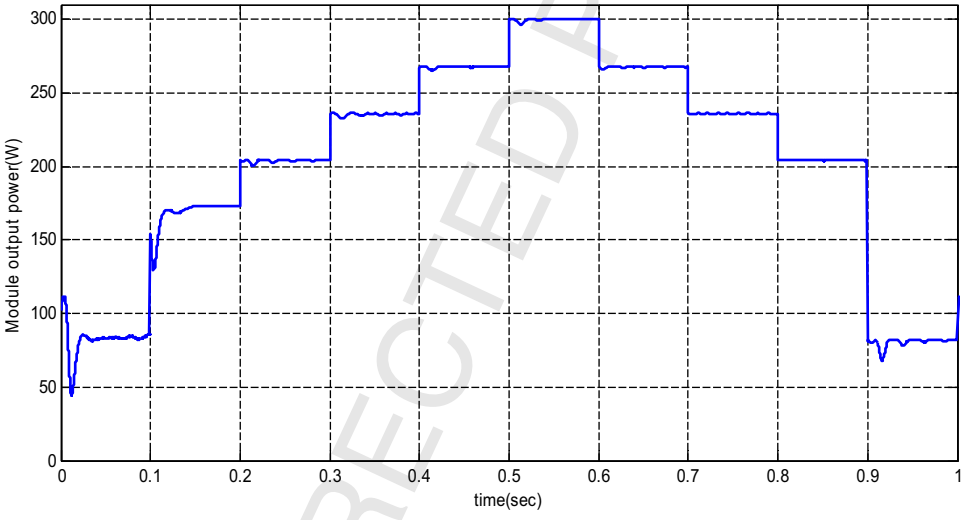

Fig. 14. Module output power through a day with MPPT using fuzzy intillegent technique.

(at point 3) which represent minimum allowable battery charging while driving the load. Also suppose the battery continue charging till reaching the maximum charging value of the upper band 100% (at point 1). In this case we should disconnect the current supplied to the batteries to protect them from overcharging by switching OFF a supposed switch (S1), and reswitching it ON again if the SOC is lower or equal to the minimum upper band 98% (at point 2) as shown in Fig. 15, and the supposed switch S2 is at ON state as shown in Fig. 16.

5. Discussion and conclusions

The standalone PV water pumping system used is described first. It consists of a PV array, a maximum power point tracking (MPPT) system controlling a DC–DC boost converter which drives a BLDC motor driving a positive displacement water pump. Two MPPT techniques are introduced P&O method and FLC method, and the two methods are compared. From the simulation results it can be noticed that FLC is faster and has lower oscillation around the maximum power point than the P&O. The battery backing system is also designed together with its control system to satisfy system requirements all the time. Simulation results presenting the system performance were presented and discussed. By apply this system in multiple or large scale system could solve the problem of water in remote areas

Please cite this article in press as: Aboul Zahab, E.E., et al., Design and control of a standalone PV water pumping system. J. Electr. Syst. Inform. Technol. (2016), http://dx.doi.org/10.1016/j.jesit.2016.03.003

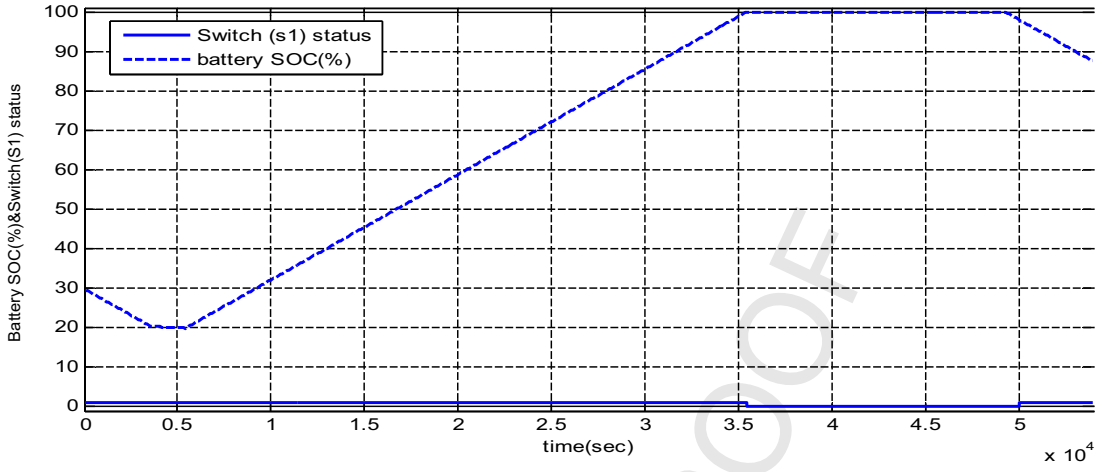

Fig. 15. Battery SOC (%) with switch (S1) status.

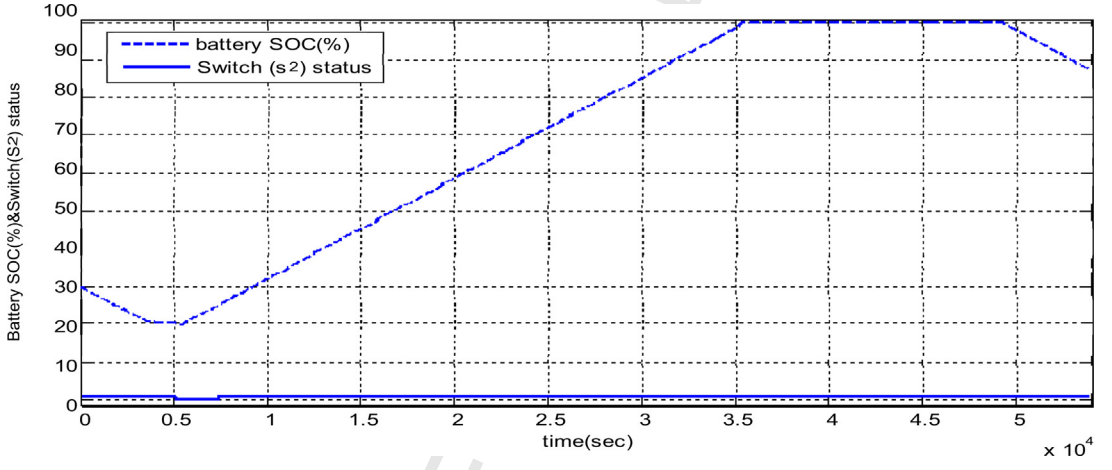

Fig. 16. Battery SOC (%) with switch (S2) status.

and could extract it for one-fifth of the world's population (about 1.2 billion people) who live in zones where water is physically rare.

Q7 Appendix A. BLDC motor parameters

Motor data	Unit	Value
Number of pair poles		1
Power rating	W	101
Nominal voltage	V	48
Rated speed	rpm	10,000
Rated torque	mNm	40
No load current	A	0.109
Terminal resistance phase to phase	Ohm	4.4
Terminal inductance phase to phase	mH	0.678
Torque constant	mNm/A	37.02
BEMF constant	mV/rpm	3.877
Rotor inertia	gcm^2	34
Friction torque	mNm/rpm	2.4×10^{-4}

Please cite this article in press as: Aboul Zahab, E.E., et al., Design and control of a standalone PV water pumping system. J. Electr. Syst. Inform. Technol. (2016), http://dx.doi.org/10.1016/j.jesit.2016.03.003

References

Aashoor, F.A.O., Robinson, F.V.P., 2013. Maximum power point tracking of photovoltaic water pumping system using fuzzy logic controller. In: IEEE 48th International Universities' Power Engineering Conference (UPEC), 2–5 September, pp. 1–5.

Armstrong, S., Glavin, M.E., Hurley, W.G., 2008. Comparison of battery charging algorithms for stand alone photovoltaic systems. In: IEEE Power Electronics Specialists Conference (PESC), 15–19 June.

Das, Bikram, Chanda, Mahua, 2014. Torque ripple reduction and speed performance of BLDCM drive with hysteresis current controller. Int. J. Eng. Res. Technol. (IJERT) 3 (May (5)), 194–201.

Elgendy, M.A., Zahawi, B., Atkinson, D.J., 2012. Evaluation of perturb and observe MPPT algorithm implementation techniques. In: 6th IET International Conference on Power Electronics, Machines and Drives, 27–29 March, pp. 1–6.

Hmidet, Ali, Gammoudi, Rabiaa, Hasnaoui, Othman, Dhifaoui, Rachid, 2014. Analog MPPT controller circuit used in photovoltaic pumping systems. In: IEEE Fifth International Renewable Energy Congress IREC Hammamet, Tunisia, 25–27 March.

Jaycar Electronics Reference Data Sheet, Choosing a Rechargeable Battery. http://www.jaycar.com/images_uploaded/recharge.pdf.

Mahmoud, Yousef, Xiao, W., Zeineldin, H.H., 2012. A simple approach to modeling and simulation of photovoltaic modules. IEEE Trans. Sustainable Energy 3 (January (1)), 185–186.

Mansour, Atef M., Faris, Khaled N., El-Din Aboul Zahab, Essam, 2015. Smart energy management controller for a micro grid. Int. J. Eng. Res. (IJER) 4 (8), 456–464.

Mohammedi, Ahmed, Rekioua, Djamila, Mezzai, Nabil, 2013. Experimental study of a PV water pumping system. J. Electr. Syst. 9 (2), 212–222.

Oi, Akihiro, 2005. Design and simulation of photovoltaic water pumping system. In: A Thesis Presented at the Faculty of California Polytechnic State University, San Luis Obispo, September.

Pillay, Pragasen, Krishnan, Ramu, 1989a. Modeling, simulation, and analysis of permanent-magnet motor drives, Part I: the permanent-magnet synchronous motor drive. IEEE Trans. Ind. Appl. 25 (March/April (2)), 265–273.

Pillay, Pragasen, Krishnan, Ramu, 1989b. Modeling, simulation, and analysis of permanent-magnet motor drives, Part II: the brushless DC motor drive. IEEE Trans. Ind. Appl. 25 (March/April (2)), 274–279.

Putta Swamy, C.L., Singh, B., Singh, B.P., 1995. Dynamic performance of a permanent magnet brushless DC motor powered by a PV array for water pumping. Sol. Energy Mater. Sol. Cells 36 (2), 187–200.

Rebhi, Mhamed, Benatillah, Ali, Sellam, Mabrouk, Kadri, Boufeldja, 2013. Comparative study of MPPT controllers for PV system implemented in the South-west of Algeria. Energy Procedia 36, 142–153.

Sanita, C.S., Kuncheria, J.T., 2013. Modelling and simulation of four quadrant operation of three phase brushless DC motor with hysteresis current controller. Int. J. Adv. Res. Electr. Electron. Instrum. Eng. (IJAREEIE) 2 (June (6)), 2461–2470.

Sreekumar, Shilpa, Benny, Anish, 2013. Maximum power point tracking of photovoltaic system using fuzzy logic controller based boost converter. In: IEEE International Conference on Current Trends in Engineering and Technology, ICCTET'13, Coimbatore, India, 3 July.

The United Nations World Water Development Report, 2015. Water for a Sustainable World. http://unesdoc.unesco.org/images/0023/002318/231823E.pdf.

Tremblay, Olivier, Dessaint, Louis-A., Dekkiche, Abdel-Illah, 2007. A generic battery model for the dynamic simulation of hybrid electric vehicles. In: IEEE Vehicle Power and Propulsion Conference, 9–12 September, pp. 284–289.

Please cite this article in press as: Aboul Zahab, E.E., et al., Design and control of a standalone PV water pumping system. J. Electr. Syst. Inform. Technol. (2016), http://dx.doi.org/10.1016/j.jesit.2016.03.003